Predictions of Enhanced Chemical Reactivity at Regions of Local Conformational Strain on Carbon Nanotubes: Kinky Chemistry

Deepak Srivastava

National Aeronautics and Space Administration (NASA), Ames Research Center, MS T27A-1, Moffett Field, California 94035-1000

Donald W. Brenner and J. David Schall

Department of Materials Science and Engineering, North Carolina State University, Raleigh, North Carolina 27695-7907

Kevin D. Ausman, MinFeng Yu, and Rodney S. Ruoff*

Department of Physics, Washington University, St. Louis, Missouri, 63130-4899

Received: March 12, 1999

Simulations that model the effects of conformational strain on the chemical reactivity of single-walled carbon nanotubes suggest a method for significantly enhancing their reactivity locally by controlled deformations. The chemisorption of hydrogen atoms is predicted to be enhanced by as much as 1.6 eV at regions of high conformational deformation, suggesting that local reactivity will be significantly enhanced. Analysis of the local electronic density of states suggests the introduction of radical p orbital character to the sites that are locally deformed, consistent with the heightened reactivity and large pyramidalization angles at these sites. Preliminary experimental data consistent with this predicted heightened reactivity is also presented.

I. Introduction

Carbon nanotubes have remarkable mechanical and electronic properties that make them likely candidates for components in molecular-scale machines and electronics.[1−8] To fully integrate these species into such devices, it will be necessary to controllably functionalize them in ways that ensure good mechanical and electrical contact between the tubes and the other components of the devices. Furthermore, controlled derivitization could even locally modify the properties of the nanotubes themselves.[9] Thus, not surprisingly, the field of carbon nanotube functionalization is growing rapidly.[10−16]

Pristine carbon nanotubes are preferentially reactive at their end caps.[12,17−19,20] This can be understood by examining the effects of curvature at these caps on the carbon atoms' orbitals.[13,21,22] This curvature leads to (a) a loss of spatial overlap of the atomic p orbitals that contribute to conjugation and (b) a shift in hybridization of the atoms from the sp^2 of graphite to something intermediate between sp^2 and sp^3. The net result of these orbital effects is an increase in energy locally and an introduction of partial radical character in the π-bonding electrons.

Addition reactions across unstrained olefins have several characteristics in common with this out-of-plane bending of three-coordinate carbon atoms. As the reactant carbon atoms shift from three to four coordinate, the local preferred geometry correspondingly shifts from planar to tetrahedral. Furthermore, any local conjugation is broken and the carbon atoms rehybridize from sp^2 to sp^3. The energy required to induce such curvature, commonly called strain energy, can therefore be considered as energy already added along the reaction coordinate for an addition reaction, thus enhancing reactivity selectively at the highly curved sites.

To date, for the reasons described above, most functionalization of carbon nanotubes has been performed at oxidatively opened end caps.[12,14,15] Although end-cap derivitization is likely to be useful in the construction of nanotube-based devices and materials, there are several aspects of these recently applied approaches that leave room for improvement. For example, because of carbon nanotubes' high aspect ratio, end-cap functionalization is unlikely to significantly affect the bulk properties of the tubes. The ability to react only at the end caps severely limits the flexibility of design schemes for molecular devices, including primarily contacts to surfaces and component interconnects. Furthermore, the oxidation methods so far employed appear to result in some small degree of functionalization along the tubes' side walls.[10,11,13,16] Thus, though the oxidation of carbon nanotubes appears to be preferential toward areas of high curvature, it is not completely selective. A method for side-wall reactivity of carbon nanotubes, based on carbene addition and Birch reduction, has recently been reported.[13,23] However, this method does not allow for site specificity, and as these reactions were performed on carbon nanotubes that did not have end caps present, it has not been proven that these reactions preferentially occur at the side walls over the end caps.

If indeed chemical reactivity in carbon nanotubes is at least partially driven by local strain, it is reasonable to suppose that local side-wall reactivity could be enhanced, perhaps significantly, by the introduction of areas of local conformational strain, such as by mechanical kinking or twisting. For example, Ruoff and LaDuca invented a method for stress-loading carbon nanotubes, by dispersing them onto Formvar-coated TEM grids, and heating the Formvar to above its thermal distortion temperature of ∼90 °C. As the thin (∼30 nm thick) Formvar film distorts, nanotubes are "caught" at their ends and compres-

10.1021/jp990882s CCC: $18.00
Published on Web 05/05/1999

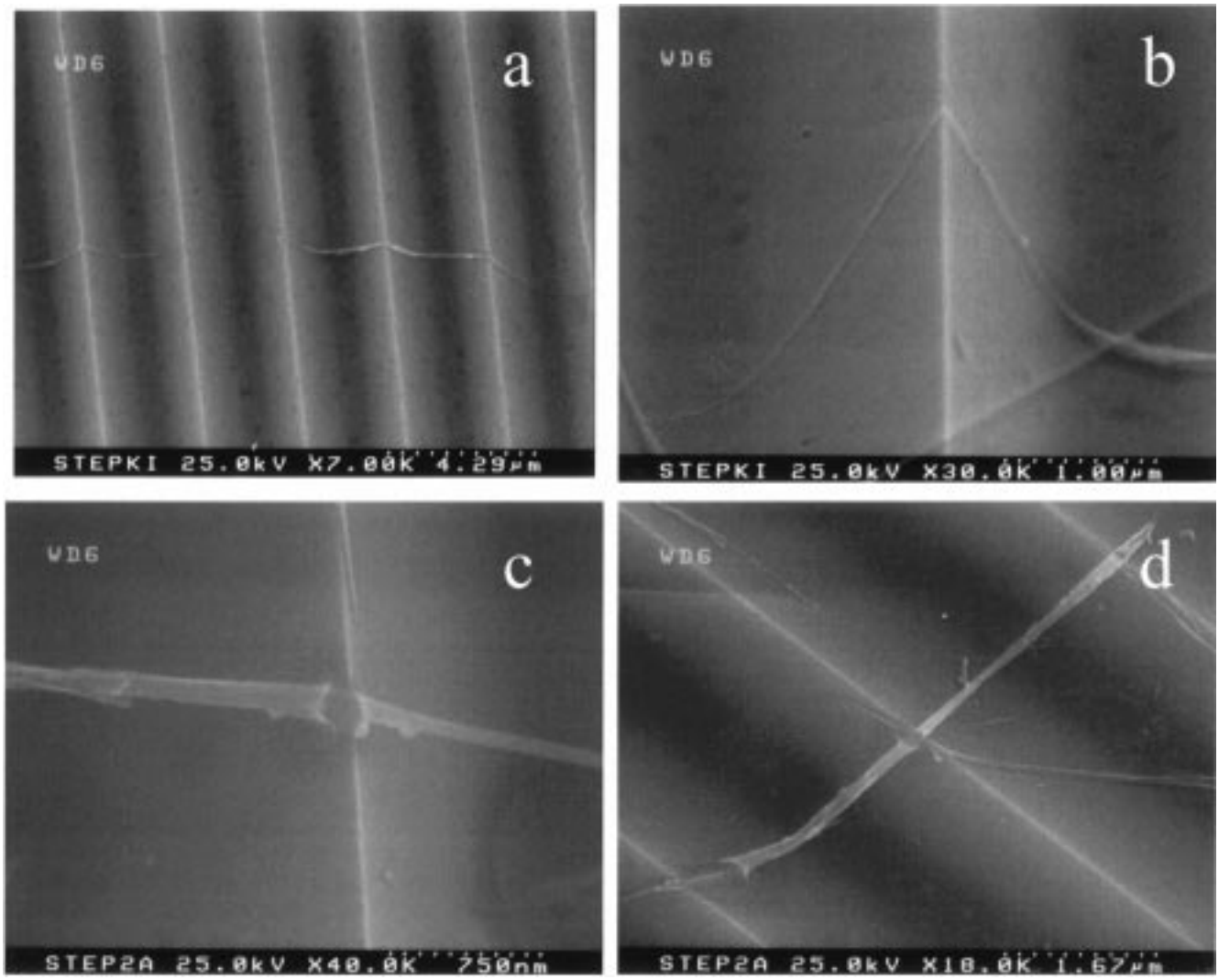

Figure 1. SEM images of multiwalled carbon nanotubes (oxidatively purified, donated by R. Smalley) dispersed on a V-ridge substrate (K-Tek TGG01; 3.0 μm apart, 1.7 μm tall, 70° peak). (a,b) Typical examples of tubes before reaction. (c,d) Typical examples of tubes in the same sample after exposure to nitric acid vapor at room temperature. Images taken on a Hitachi S-4500 field emission gun SEM. No effort was made in this preliminary experiment to image the same tubes before and after exposure to nitric acid vapor.

sively stress loaded, and subsequently imaged by high-resolution TEM.[24−26] Such areas of high conformational strain have also been observed in high-resolution transmission electron micrographs of both single- and multiwall nanotubes by others.[1,27] The observed kinking behavior is thought to be an elastic conformational deformation rather than a plastic isomerization,[3,4] so after performing the kink-catalyzed chemical reaction, or "kinky chemistry," it should be possible to straighten the tube, leaving a selectively side-wall functionalized carbon nanotube. This represents a new way of doing chemistry. The use of new tools soon, which may controllably deform carbon nanotubes as well as other structures that could be stressed-loaded and locally deformed such as individual graphite sheets, will allow for the detailed experimental testing of the theoretical results presented below, and should lead to important applications as well.

It is important in this discussion to clearly distinguish two different sources of curvature in carbon nanotubes, nonhexagonal defects, and conformational strain. The former, whether present along the side of an imperfect nanotube or inducing the curvature at an end cap, will locally raise energy relative to planar carbon under all conditions. The latter is elastic, and with the aid of various nanomanipulation techniques could be controllably and reversibly introduced. Finally, as is evident from the figures in this work, curvature from conformational strain can greatly exceed that produced by pentagonal or heptagonal defects, thus likely enhancing reactivity significantly beyond that at the topological imperfections. With this ability to tailor reaction energetics by externally introduced mechanical stresses, it should be possible to optimize reaction conditions to selectively perform desired reactions at kinks only, and thus at any specific desired sites along a carbon nanotube.

The plausibility of this concept of kink-promoted chemistry is consistent with our recent experimental results on multiwall carbon nanotube bundles dispersed on a V-ridge surface (Figure 1 a,b). As can be clearly seen, the nanotubes closely follow the surface and exhibit a high degree of local curvature at the peaks of the ridges. These dispersed nanotube bundles were then exposed to room temperature nitric acid vapor for several hours. The kinked regions were attacked by the acid vapor, as is evident in Figure 1c,d. As expected, the acid etching did not propagate down the length of the tube, because of the low reaction temperature. The tubes shown are typical examples. Similar etching was not observed at sites away from the ridge-induced kinks. We do not consider this evidence to conclusively prove the concept of kink-promoted chemistry, but rather to suggest

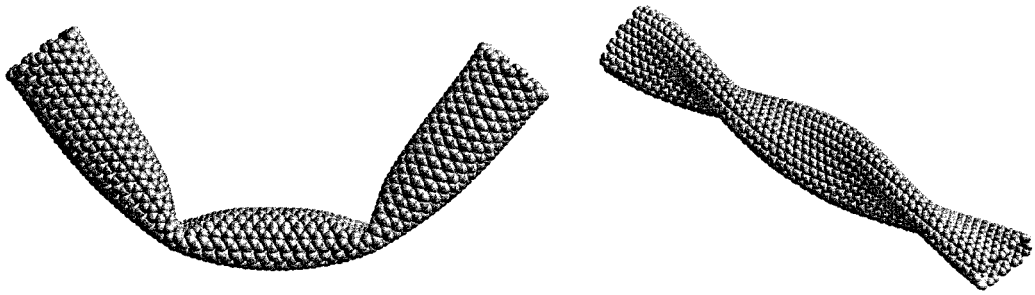

Figure 2. Illustrations of nonlinear distortions in strained single-wall (10,10) carbon nanotubes. Left: Kinks in a bent nanotube. Right: Ribbon structure resulting from torsional strain.

its reasonableness in support of the theoretical predictions presented here. Experiments in progress include the controlled deformation, in the presence of reactive species, of both multiwall and single-wall carbon nanotubes. Controlled deformation of individual tubes can be achieved by methods such as proximal probe tip force application and by a new nanostressing stage under construction in the Ruoff group and of bulk quantities of tubes by ultrasonic cavitation in solution or suspension.

In this paper, results are reported below from calculations carried out to analyze how local nonlinear distortions in strained carbon nanotubes may act as sites for enhanced chemical reactivity as suggested by the experiment described above. Two types of nonlinear distortions of single-walled (10,10) nanotubes are considered; "kinks" resulting from bending (Figure 2, left) and "ridges" resulting from torsional strain (Figure 2, right). Binding energies and reactive dynamics of hydrogen atoms calculated using a many-body analytic bond-order potential are used as a measure of reactivity. The calculations predict that chemisorption energies may be enhanced by as much as 1.6 eV relative to unstrained carbon nanotubes for specific sites associated with the nonlinear distortions. This indicates enhanced chemical reactivity at these sites. Analysis of the electronic local density of states at these sites calculated from a tight-binding model suggests the formation of radical p orbitals associated with kinks that are removed by hydrogen chemisorption. A π-orbital axis vector (POAV) analysis,[21,28,29] which is used to quantify local strain in the deformed structures, shows a positive correlation between enhanced chemical reactivity and values of POAV pyramidalization angles at the locally deformed sites.

II. Computational Methods

The analytic potential is a variation of the second moment approximation to the local electronic density of states.[30,31] It models the potential energy of a collection of atoms as a sum of interatomic repulsive and attractive pair terms. The latter, which represent bonding from valence electrons, are modulated by many-body empirical bond-orders that are a function of local coordination, bond angles, radical character, and π-bond conjugation. The original form of the potential was developed to model the vapor deposition of diamond films,[30] although it has found considerable use in modeling fullerenes.[32−35] The function used here is similiar in form to that in Brenner,[30] with modifications that produce an improved description of the elastic properties of diamond and graphite.[36]

The nonlinear distortions in the single-wall (10,10) carbon nanotubes were generated as follows. To form "kinks", 100 atoms at each end of a nanotube 12 nm long containing 2000 atoms were deformed such that the nanotube was bent by 5°. Holding the end atoms rigid, the positions of the remaining atoms were relaxed to the minimum energy structure predicted by the empirical potential. These atoms were then held rigid, and the relative coordinates of the end atoms were relaxed to obtain their lowest energy configuration. This procedure was repeated until a bending angle of approximately 90° was obtained. This process resulted in the formation of two localized kinks as illustrated at the left of Figure 2. The torsional strain was carried out by twisting 160 atoms at each end of a 34 nm long nanotube at a rate of one full circle per 20 ps while allowing the remaining atoms to equilibrate using molecular dynamics and the interatomic forces given by the empirical potential. The resulting ribbonlike structure is illustrated at the right of Figure 2.

The cohesive energy for an atom given by the bond-order potential is defined as one-half the sum of the pair potentials (including the modulation of the attractive terms by the empirical bond orders) between the atom and its neighbors. With this definition, the total potential energy is the sum of the atomic cohesive energies. The relative cohesive energies reported below are referenced to the cohesive energy of carbon atoms in an undistorted nanotube. Positive values correspond to atoms that are more weakly bound than those in the undistorted nanotubes.

Chemisorption of atomic hydrogen was modeled by placing a hydrogen atom near a selected site in the structures illustrated in Figure 2, keeping the carbon atoms at the ends of the nanotubes rigid, and relaxing the remaining atomic coordinates to the minimum energy given by the bond-order function. The binding energy for a given site is defined as the difference between the total energy of the distorted nanotube with and without the hydrogen atom. The relative binding energies reported below are referenced to chemisorption of single hydrogen atoms to an undistorted nanotube such that negative values correspond to sites at which hydrogen atoms are more strongly bound than they would be on undistorted nanotubes.

In addition to the static calculations, classical trajectory simulations of hydrogen atoms colliding with a six nanometer long section from the center of the torsionally strained nanotube were carried out. These were performed by first holding the 62 atoms at the two ends of the nanotube section rigid while equilibrating the remaining atoms to 300 K for 2 ps. A total of 500 hydrogen atoms were then added to the system by randomly placing them on the surface of an imaginary cylinder positioned axially around the nanotube and giving them a thermal distribution of atomic velocities at 300 K pointing into the center of the cylinder (Figure 3a). Trajectories of the atoms were then followed for 10 ps, orders of magnitude longer than a typical C−H stretching vibrational period, by numerically integrating classical equations of motion using interatomic forces from the bond-order potential (Figure 3b,c). During this process, a square periodic boundary condition in the plane normal to the axis of the tube keeps all the unreacted H atoms and molecules within the vicinity of the torsionally distorted tube.

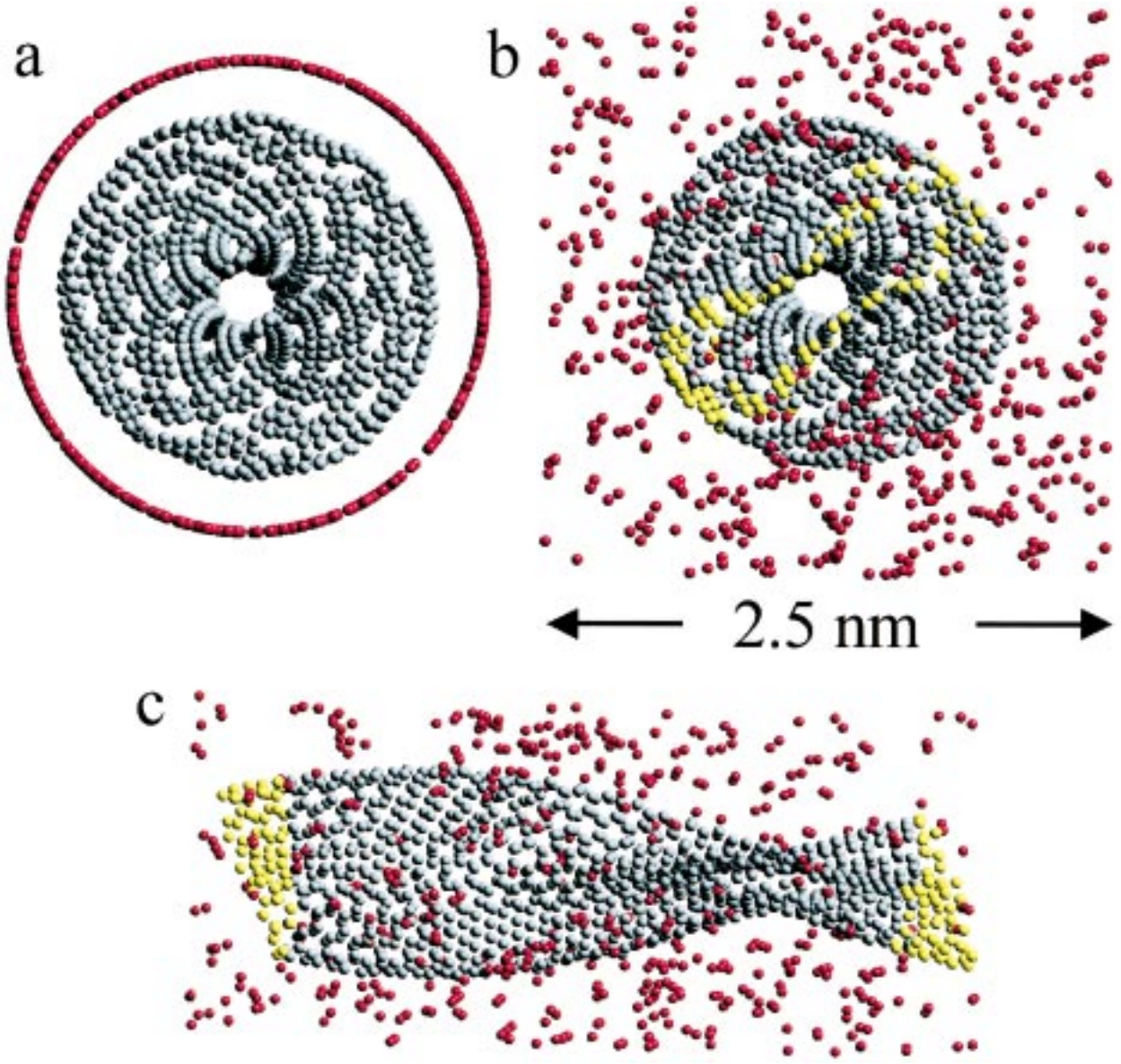

Figure 3. Illustration of the steps used in the classical trajectory calculations. (a) Initial nanotube with hydrogen atom positions initialized along the surface of a cylinder. (b) End view during the simulation. The arrow indicates the scale of the periodic bounding box. (c) Side view during the simulation.

To help validate the empirical potential calculations, and to lend insight into the electronic origins of the results, tight-binding calculations using a valence s−p basis were carried out on strained and unstrained nanotubes using the structures predicted by the empirical potential. The tight-binding parametrization is due to White and co-workers;[37,38] it was fit to the electronic properties of electroactive polymers and first-principles predictions of carbon nanotube band gaps. Values for the hopping integrals were assumed to follow the $1/d^2$ behavior suggested by Harrison[39] where d is the interatomic distance between neighboring atoms. The local electronic energy for each atom is defined as twice the sum of the occupied molecular orbitals weighted by the local density of states. With this definition, the total electronic energy, given by twice the sum of occupied molecular orbitals, is the sum of the local electronic energies. The relative local electronic energies reported below are referenced to those for an undistorted nanotube such that negative values correspond to atoms that are more electronically stable. The results presented here were calculated with a finite length nanotube segment, and so the resulting electronic density of states (DOS) near the Fermi region are somewhat different from the standard DOS reported for a (10,10) nanotube with no edges or dangling bonds at the edges. This is justified because our main purpose is to study only the changes in the DOS of an undistorted nanotube as a function of local conformational strain and H atom reaction at the strained sites.

POAV1 pyramidalization angle is a particularly straightforward parametrization of the deviation from planarity of conjugated carbon atoms, and thus provides a simple estimation of local strain.[28] In this analysis, the π-orbital axis vector (POAV1) is defined as the vector that makes equal angles with the three bonds of the carbon atom. For simplicity, the pyramidaliation angle is defined as this angle minus 90°. Because the local curvature is directional, and chemisorption is only examined from the outside of the nanotubes, we define the pyramidalization angle as positive for convex carbon sites, and negative for concave sites.

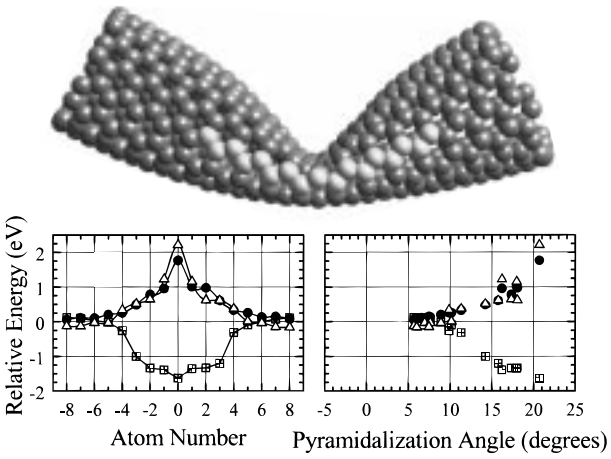

Figure 4. Structures and energies for the first set of high-symmetry binding sites considered for the bent nanotube. Top: Close-up of the kink. The highlighted atoms denote the binding sites. Bottom left: Relative hydrogen atom binding energies (squares), relative cohesive energies (circles), and relative electronic energies (triangles) for the highlighted atoms. The center atom along the line of highlighted atoms illustrated at the left of the figure corresponds to an abscissa equal to zero. Bottom right: Dependence of these energies on POAV1 pyramidalization angle.

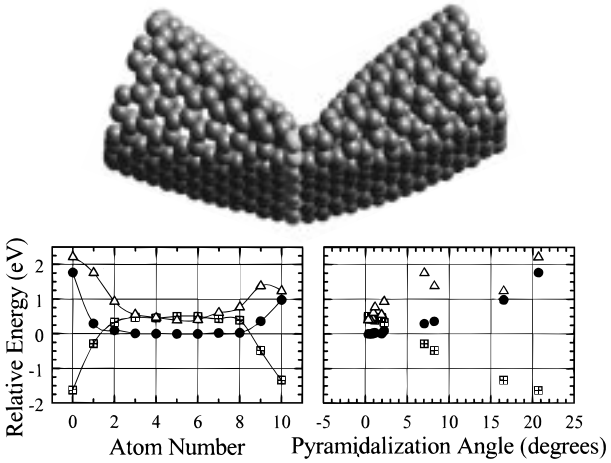

Figure 5. Structures and energies for the second set of high-symmetry binding sites considered for the bent nanotube. Top: Close-up of the kink. The highlighted atoms denote the binding sites. Bottom left: Relative hydrogen atom binding energies (squares), relative cohesive energies (circles), and relative electronic energies (triangles) for the highlighted atoms. Bottom right: Dependence of these energies on POAV1 pyramidalization angle.

III. Results

Detailed illustrations of the kinks formed in the bent (10,10) carbon nanotube are presented at the left of Figures 4 and 5. The outer regions of the kinks, which are in tension, are slightly flattened relative to the unstrained structure. The inside of the kinks are in compression; this results in a "fold" in the structure toward the inside of the nanotube. The radius of the nanotube parallel to the direction of the fold is elongated relative to the radius of the initial, unstrained structure. This structure is consistent with prior simulations, continuum theory, and experimental observations.[1,3,40,41] A close-up view of the ribbonlike structure resulting from torsional strain is illustrated in Figure 6. There are two distinct regions present in this structure. The first is a flat region where opposite walls of the nanotube approach one another in a parallel configuration. The separation between these walls is determined by the degree of strain and

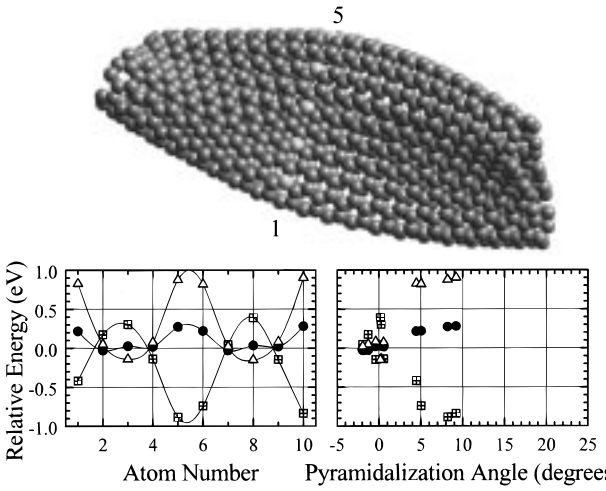

Figure 6. Structures and energies for the binding sites considered on the torsionally strained nanotube. Top: Close-up of the nanotube. Five of the ten binding sites, denoted by the highlighted atoms, are visible. The remaining sites are on the backside of the nanotube. Bottom left: Relative hydrogen binding energies (squares), relative cohesive energies (circles), and relative electronic energies (triangles) for the highlighted atoms. The sites indicated on the abscissa by 5-6 and 10-1 correspond to the ribbon edges, while the remaining sites are on the flat regions of the nanotube. Bottom right: Dependence of these energies on POAV1 pyramidalization angle.

the interatomic interactions. The second region, which contains relatively sharp curves, is where the edges of the flat regions are connected.

Two sets of high-symmetry binding sites were considered for hydrogen chemisorption to the bent nanotube. The first, indicated by the highlighted atoms in the illustration at the top of Figure 4, is along the top of a kink parallel to the nanotube axis. This line separates regions of hydrostatic compressive and tensile stress, and therefore the atoms are under an approximately zero hydrostatic stress. Relative binding energies for single hydrogen atoms chemisorbed at each of these sites are given by the squares in the plot at the bottom left of Figure 4. The center of the plot (abscissa equal to 0) corresponds to the carbon atom at the center of the kink. This site, which is raised above the line of atoms away from the center of the nanotube, has a binding energy for hydrogen that is 1.6 eV more stable than that for the undistorted nanotube. Indicated in the plot by the circles and triangles are the relative atomic cohesive energies and relative local electronic energies, respectively, for the distorted nanotube before chemisorption. The trends given by the bond-order potential and tight-binding calculations show good agreement. For this set of atoms, enhanced reactivities, as measured by the hydrogen binding energies, correspond to sites where carbon atoms have relatively weakened potential energies due to the nonlinear distortions within the bent nanotube.

Illustrated at the top of Figure 5 by the highlighted atoms is the second set of high-symmetry sites considered in the calculations. These correspond to chemisorption at the outside of a kink along a line perpendicular to the nanotube axis. Indicated by the squares in the plot in the bottom left of Figure 5 are the relative hydrogen binding energies along these sites. Also given in this plot are the relative atomic cohesive energies (indicated by the circles) and the relative local electronic energies (indicated by the triangles) for the carbon atoms at these sites prior to chemisorption. The initial point on the plot (abscissa equal to 0) corresponds to the center point in the structure illustrated at the left of Figure 4. The kink, as predicted

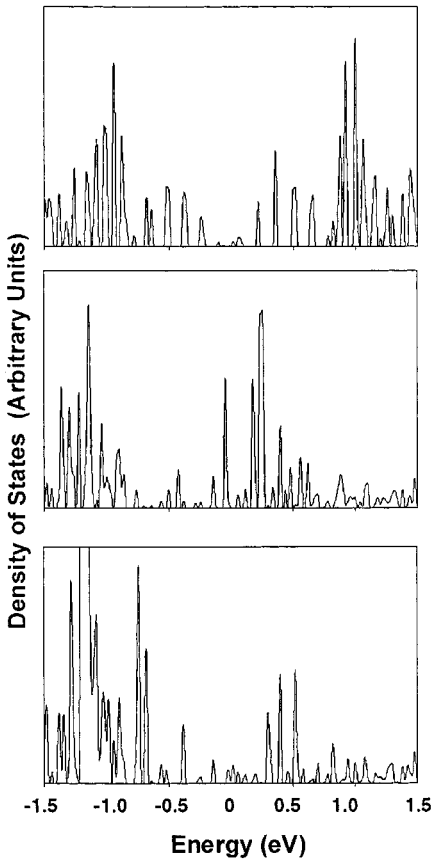

Figure 7. Local electronic density of states from the tight-binding model for the reactive carbon atom at the top of the kink discussed in the text. The Fermi energy is at zero. Top: Unstrained nanotube. Middle: Bent nanotube before hydrogen chemisorption. Bottom: Bent nanotube after hydrogen chemisorption to this site.

by the method outlined above, is not completely symmetric about the nanotube axis, but rather has a single-atom offset from the top to the bottom of the kink. This results in the asymmetry apparent from the values plotted in Figure 5. The raised atom at the top of the kink represents a site of relatively destabilized cohesive and local electronic energy, and high chemical reactivity, consistent with the first set of calculations.

Chemisorption of hydrogen atoms at a line of sites along the fold at the inside of the kink was also attempted. In this case, significant chemical bond formation between the carbon and hydrogen atoms (as determined by bond lengths) correlated strongly with complete breaking of carbon−carbon bonds. The resulting configurations were relatively high in energy. Chemisorption to the inside of the nanotube along these sites was not explored.

Plotted in Figure 7 are the electronic local density of states from the tight-binding model for the reactive carbon atom at the top of the kink discussed above. The top plot corresponds to a finite unstrained (10,10) nanotube segment, while the middle and bottom plots correspond to the atom in the bent nanotube segment of the same length before and after hydrogen chemisorption to this site, respectively. There is a peak in the local density of states at the Fermi energy (energy equal to zero) in the center plot that is not present in the unstrained nanotube and that disappears with hydrogen chemisorption. This is consistent with the formation of a radical p orbital on the reactive atom caused by the kink that is removed by hydrogen chemisorption.

Binding energies were examined for 10 sites on the torsionally strained nanotube around the nanotube circumference. Five of these are indicated by the highlighted atoms in the illustration at the top of Figure 6, with the other five on the backside of the nanotube (and hence not visible in the figure). Sites 5-6 and 10-1 correspond to the ribbon edges, while the remaining sites are on the relatively flat regions of the nanotube. Indicated in the plot at the bottom left of Figure 6 by the squares, circles and triangles are the relative hydrogen-atom binding energies, relative atomic cohesive energies, and relative local electronic energies, respectively, for these sites. The asymmetry in the curves is due to the asymmetry in the structure of the deformed nanotube. The correlation between the electronic, cohesive and hydrogen binding energies is as described above for the kink in the bent nanotube. The hydrogen binding at the edge sites is about 1 eV more stable than that on an undistorted nanotube and about 1.5 eV more stable than the sites in the flat region of the distorted nanotube. The large nonlinear distortions thus create stronger chemisorption reactivity and relatively weaker cohesive and electronic energies at the ribbon edges. This suggests that the edge regions are susceptible to stronger chemical attack relative to an unstrained nanotube.

For all three sets of sites reported in Figures 4−6, the hydrogen-atom binding energies show a strong correlation with pyramidalization angle, as is shown by the squares in the bottom right plot of each figure. In the torsionally strained case, shown in Figure 6, the correlation in the flat region of the ribbonlike strained tube is less clear because both locally positive and negative pyramidalization angles are possible and observed. The strong positive correlation in the relative energies of the edge region and pyramidalization angles, however, is the same as that of the kinked tube in Figures 4 and 5. An additional contributing effect may be a greater contribution of local bond torsion leading to greater p-orbital isolation, an effect not considered by the POAV1 approximation.[42] Similar strong correlations are observed between pyramidalization angle and relative atomic cohesive energies, and to a lesser extent the relative local electronic energies, shown as circles and triangles, respectively. Though POAV1 analysis is significantly less sophisticated a computational approach than the other methods presented here, these strong correlations supports the notion that chemical reactivity is heightened by local conformational deformations, and provides an extremely simple rule-of-thumb for determining relative reactivity in strained, conjugated carbon systems, such as conformationally strained carbon nanotubes.

As examples of the enhanced chemisorption reactivity at the ribbon edges, structures resulting from two of the classical MD trajectory simulations are illustrated in Figure 8. For clarity, all of the nonreacted gas-phase H atoms and molecules have been removed from the system. Apparent from the figure is that the carbon atoms at the edges of the ribbons are more susceptible to hydrogen chemisorption than those along the flat regions of the nanotube. This difference in reactivity is consistent with the static energy calculations described above. The ratio of hydrogen atoms reacting with the carbon atoms at the ribbon edges to those reacting at the flat regions of the nanotube is approximately 5:1. Although more trajectories are required to determine quantitative differences in the rates, the areas of high local nonlinear strain clearly represent regions of enhanced reactivity. From the high degree of selectivity shown here, it is clear that the reaction barrier to chemisorption is small compared to kT at 300 K.

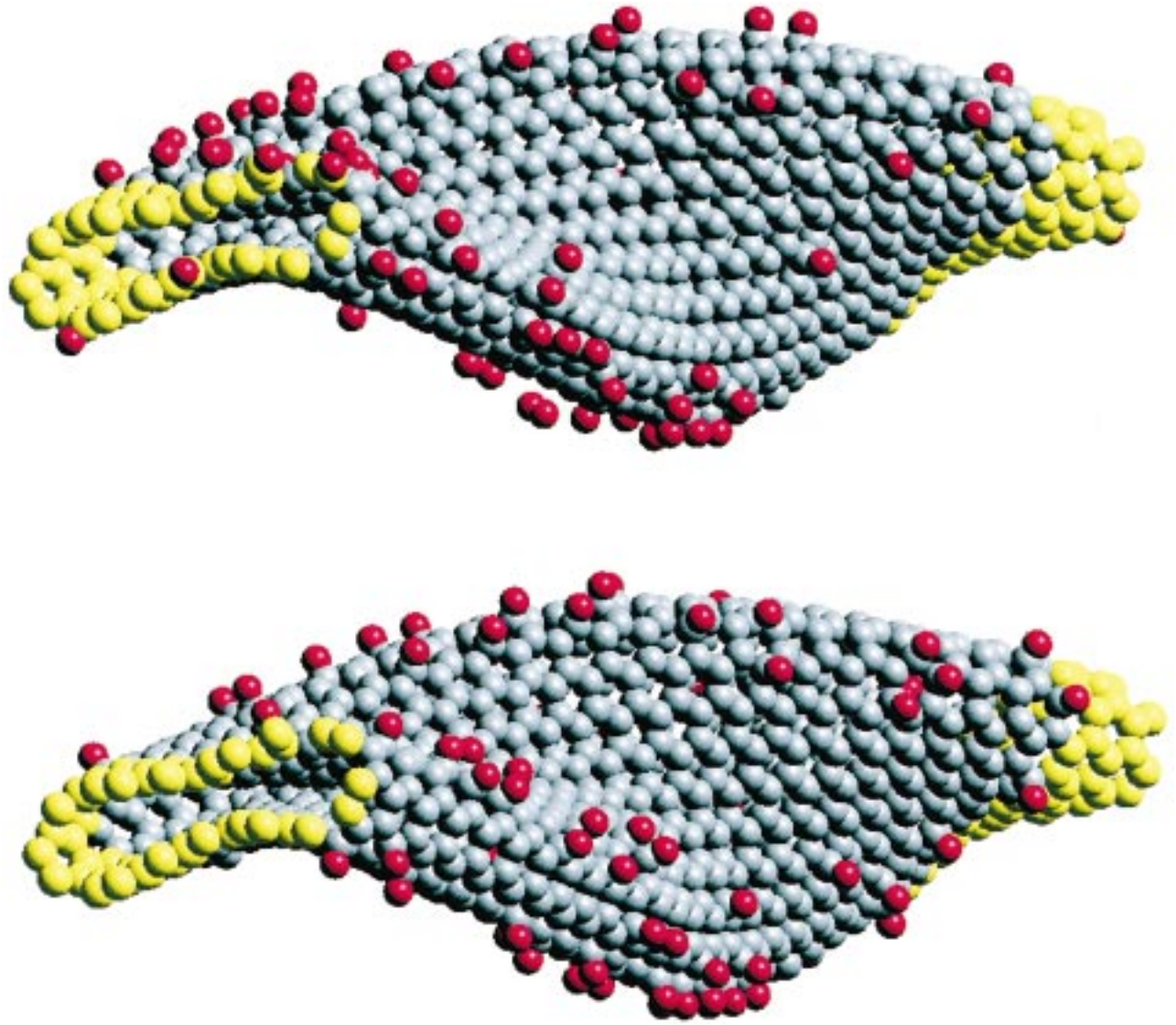

Figure 8. Final structures from two of the classical trajectory simulations. For clarity, all of the unreacted gas-phase H atoms and molecules have been removed.

IV. Conclusions

Estimates for energies of a hydrogen atom chemisorbed to sites near regions of local nonlinear distortions arising from bending and torsional strain of single-wall carbon nanotubes were obtained using an analytic many-body bond-order potential. Enhanced binding relative to unstrained nanotubes is predicted for specific sites near the distortions. Analyses of atomic cohesive energies, local electronic energies and local electronic density of states from tight-binding calculations show that the sites with predicted enhanced binding energies correspond to destabilized cohesive energies and electronic states with energies near the Fermi level. These trends correlate strongly with pyramidalization angle, a simple parametrization of local strain. Classical trajectory calculations of atomic hydrogen reacting with a torsionally strained nanotube further suggest that nonlinear distortions create regions of enhanced reactivity. The correlation between the tight-binding results and the molecular dynamics results supports the accuracy and relevance of the empirical potential used in this study.

These calculations have important implications for understanding and controlling the chemistry of highly distorted carbon nanotubes. First, they suggest that kinks and other nonlinear distortions may act as sites of enhanced chemical reactivity. Although the results presented here are for atomic hydrogen, they also likely to apply (to some extent) to other reactive species. The depleted cohesive energies at the kinks and ridges also imply that oxidation may be enhanced at these sites (see for example in Figure 1). This implies that such sites might compromise the chemical integrity of a nanotube. On the other hand, this might be useful for enhancing reactivity of nanotubes via local agitation in polymer solution to make composites, and for deliberately introducing kinks (using an atomic-force microscope, for example) to control chemical addition or induce chemically enhanced fracture at specific locations along a nanotube. The correlation between less stable relative atomic cohesive and electronic energies with sites of enhanced binding suggest that reasonable predictions of reactive sites can be made for all-carbon strained nanotubes without having to explicitly consider hydrogen or other reactive species. Finally, the local energetic destabilization and thus the heightened reactivity resulting from local conformational distortions can be predicted qualitatively in a computationally nonintensive manner by examination of POAV pyramidalization angles.

This "kinky chemistry" represents a new way of doing chemistry, and the results presented here serve to challenge the experimentalist to invent methods to controllably deform carbon

nanotubes, and other unique structures (such as the graphene sheet) which could be manipulated in the presence of a range of reagents, and to further test the theoretical predictions presented here.

Acknowledgment. Part of this work (D.S.) is supported by NASA Contract NAS2-14303 to MRJ Technology. D.W.B. is supported by the NASA−Ames Computational Nanotechnology Program, a Multi-University Research Initiative of the Office of Naval Research through the North Carolina Center for Nanoscale Materials, and the National Science Foundation. Part of this work (K.D.A., M.F.Y., and R.S.R.) was partially supported by the NSF contract "New Methods and Tools for Nanotechnology," DMR Grant 9871874.

References and Notes

(1) Iijima, S.; Brabec, C.; Maiti, A.; Bernholc, J. *J. Chem. Phys.* **1996**, *104*, 2089−2092.
(2) Treacy, M. M. J.; Ebbesen, T. W.; Gibson, J. M. *Nature* **1996**, *381*, 678−680.
(3) Falvo, M. R.; Clary, G. J.; Taylor, R. M.; Chi, V.; Brooks, F. P.; Washburn, S.; Superfine, R. *Nature* **1997**, *389*, 582−584.
(4) Wong, E. W.; Sheehan, P. E.; Lieber, C. M. *Science* **1997**, *277*, 1971−1975.
(5) Charlier, J. C.; Issi, J. P. *Appl. Phys. A* **1998**, *67*, 79−87.
(6) Cornwell, C. F.; Wille, L. T. *J. Chem. Phys.* **1998**, *109*, 763−767.
(7) Frank, S.; Poncharal, P.; Wang, Z. L.; de Heer, W. A. *Science* **1998**, *280*, 1744−1746.
(8) Kasumov, A. Y.; Bouchiat, H.; Reulet, B.; Stephan, O.; Khodos, II.; Gorbatov, Y. B.; Colliex, C. *Europhysics Lett.* **1998**, *43*, 89−94.
(9) Brenner, D. W.; Schall, J. D.; Shenderova, O. A. 199. Submitted for publication.
(10) Lago, R. M.; Tsang, S. C.; Lu, K. L.; Chen, Y. K.; Green, M. L. H. *J. Chem. Soc., Chem. Commun.* **1995**, 1355−1356.
(11) Ebbesen, T. W. *J. Phys. Chem. Solids* **1996**, *57*, 951−955.
(12) Satishkumar, B. C.; Govindaraj, A.; Mofokeng, J.; Subbanna, G. N.; Rao, C. N. R. *J. Phys. B*; *At. Mol. Opt. Phys.* **1996**, *29*, 4925−4934.
(13) Chen, J.; Haddon, R. C.; Fang, S.; Rao, A. M.; Lee, W. H.; Dickey, E. C.; Grulke, E. A.; Pendergrass, J. C.; Chavan, A.; Haley, B. E.; Smalley, R. E. *J. Mater. Res.* **1998**, *13*, 2423−2431.
(14) Liu, J.; Rinzler, A. G.; Dai, H. J.; Hafner, J. H.; Bradley, R. K.; Boul, P. J.; Lu, A.; Iverson, T.; Shelimov, K.; Huffman, C. B.; Rodriguez-Macias, F.; Shon, Y. S.; Lee, T. R.; Colbert, D. T.; Smalley, R. E. *Science* **1998**, *280*, 1253−1256.
(15) Wong, S. S.; Joselevich, E.; Woolley, A. T.; Cheung, C. L.; Lieber, C. M. *Nature* **1998**, *394*, 52−55.
(16) Yu, R. Q.; Chen, L. W.; Liu, Q. P.; Lin, J. Y.; Tan, K. L.; Ng, S. C.; Chan, H. S. O.; Xu, G. Q.; Hor, T. S. A. *Chem. Mater.* **1998**, *10*, 718−722.
(17) Ajayan, P. M.; Ebbesen, T. W.; Ichihashi, T.; Iijima, S.; Tanigaki, K.; Hiura, H. *Nature* **1993**, *362*, 522−525.
(18) Tsang, S. C.; Harris, P. J. F.; Green, M. L. H. *Nature* **1993**, *362*, 520−522.
(19) Tsang, S. C.; Chen, Y. K.; Harris, P. J. F.; Green, M. L. H. *Nature* **1994**, *372*, 159−162.
(20) Sloan, J.; Hammer, J.; Zwiefka-Sibley, M.; Green, M. L. H. *Chem. Commun.* **1998**, 347−348.
(21) Haddon, R. C. *Science* **1993**, *261*, 1545−1550.
(22) Haddon, R. C.; Raghavachari, K. *Tetrahedron* **1996**, *52*, 5207−5220.
(23) Chen, J.; Hamon, M. A.; Hu, H.; Chen, Y.; Rao, A. M.; Eklund, P. C.; Haddon, R. C. *Science* **1998**, *282*, 95−98.
(24) Also, see: http://bucky5.wustl.edu/Old.nanogallery/The_Nanogallery for a detailed description of stress-loading of MWNTs by thin Formvar polymer films, and HR-TEM images of buckled and kinked MWNTs resulting from such loading.
(25) Ruoff, R. S.; Lorents, D. C.; Laduca, R.; Awadalla, S.; Weathersby, S.; Parvin, K. Nanotubes: Bending and filling: Part I. Fullerenes: Recent Advances in the Chemistry and Physics of Fullerenes and Related Materials, Reno, NV, 1995.
(26) Subramoney, S.; Ruoff, R. S.; Laduca, R.; Awadalla, S.; Parvin, K. Nanotubes: Bending and filling: Part II. Fullerenes: Recent Advances in the Chemistry and Physics of Fullerenes and Related Materials, Reno, NV, 1995.
(27) Kuzumaki, T.; Hayashi, T.; Ichinose, H.; Miyazawa, K.; Ito, K.; Ishida, Y. *Philos. Mag. A* **1998**, *77*, 1461−1469.
(28) Haddon, R. C. *Acc. Chem. Res.* **1988**, *21*, 243−249.
(29) Haddon, R. C. *J. Am. Chem. Soc.* **1997**, *119*, 1797−1798.
(30) Brenner, D. W. *Phys. Rev. B* **1990**, *42*, 9458−9471.
(31) Brenner, D. W.; Shenderova, O. A.; Areshkin, D. A. Quantum-Based Analytic Interatomic Forces and Materials Simulation. In *Reviews in Computational Chemsitry*; Lipkowitz, K. B., Boyd, D. B., Eds.; VCH Publishers: New York. In press.
(32) Mowrey, R. C.; Brenner, D. W.; Dunlap, B. I.; Mintmire, J. W.; White, C. T. *J. Phys. Chem.* **1991**, *95*, 7138−7142.
(33) Robertson, D. H.; Brenner, D. W.; Mintmire, J. W. *Phys. Rev. B* **1992**, *45*, 12592−12595.
(34) Robertson, D. H.; Brenner, D. W.; White, C. T. *J. Phys. Chem.* **1992**, *96*, 6133−6135.
(35) Dunlap, B. I.; Brenner, D. W.; Schriver, G. W. *J. Phys. Chem.* **1994**, *98*, 1756−1757.
(36) Brenner, D. W.; Shenderova, O. A.; Stuart, S.; Harrison, J. A.; Sinnott, S. B. Manuscript Unpublished.
(37) Elert, M. L.; White, C. T.; Mintmire, J. W. *Mol. Cryst. Liq. Cryst.* **1985**, *125*, 329.
(38) White, C. T.; Robertson, D. H.; Mintmire, J. W. *Phys. Rev. B* **1993**, *47*, 5485−5488.
(39) Harrison, W. A.. *Electronic Structure and Properties of Solids*; Freeman: San Francisco, 1980.
(40) Yakobson, B. I.; Brabec, C. J.; Bernholc, J. *Phys. Rev. Lett.* **1996**, *76*, 2511−2514.
(41) Srivastava, D.; Barnard, S. Molecular dynamics simulations of large scale carbon nanotubes on a shared memory architecture. IEEE SuperComputing ′97 (CDROM Version), 1997.
(42) Weedon, B. R.; Haddon, R. C.; Spielmann, H. P.; Meier, M. S. *J. Am. Chem. Soc.* **1999**, *121*, 335−340.